Fluctuation Stabilization of the *Fddd* Network Phase in Diblock, Triblock, and Starblock Copolymer Melts

Mark W. Matsen,[1,2,3,*] Thomas M. Beardsley,[1] and James D. Willis[2]

[1]*Department of Chemical Engineering,*
University of Waterloo, Waterloo, Ontario N2L 3G1, Canada

[2]*Department of Physics & Astronomy,*
University of Waterloo, Waterloo, Ontario N2L 3G1, Canada

[3]*Waterloo Institute for Nanotechnology,*
University of Waterloo, Waterloo, Ontario N2L 3G1, Canada

Abstract

Self-consistent field theory has demonstrated that the homologous series of $(AB)_M$ starblock copolymers are promising architectures for the complex network *Fddd* phase. Nevertheless, it remains to be seen if the level of segregation will be sufficient to survive the fluctuations inevitably present in experiments. Here, we study the effect of fluctuations using field-theoretic simulations, which are uniquely capable of evaluating order-order phase transitions. This facilitates the calculation of complete fluctuation-corrected diagrams for the diblock ($M = 1$), symmetric triblock ($M = 2$), and 9-arm starblock ($M = 9$) architectures. Although fluctuations disorder the *Fddd* phase at weak segregations, they also stabilize the *Fddd* phase with respect to its ordered neighbors, which extends the *Fddd* region to higher segregation. Our results provide strong evidence that *Fddd* will remain stable in experiments on the side of the phase diagram where the outer *A* blocks of the star form the network domain. However, it is doubtful that *Fddd* will survive fluctuations on the other side where they form the matrix domain.

(September 27, 2023)

INTRODUCTION

Two decades have passed since the initial discovery of the $Fddd$ network phase in ABC triblock terpolymer melts [1–4]. Shortly after the discovery, Tyler and Morse [5] predicted its stability using self-consistent field theory (SCFT). Interestingly, they found that the $Fddd$ region extends to the binary limit corresponding to AB diblock copolymer melts, although only for $\chi N \leq 13.7$ [6], where χ is the Flory-Huggins interaction parameter and $N = N_A + N_B$ is the total polymerization. Given the relatively weak segregation, Tyler and Morse suggested that $Fddd$ would likely be destroyed by fluctuations, which are controlled by the invariant polymerization index

$$\bar{N} = a^6 \rho_0^2 N, \tag{1}$$

where a is an average statistical segment length and ρ_0 is the bulk segment density. Indeed, using Landau-Brazovskii theory [7], Miao and Wickham [8] predicted $Fddd$ to be unstable for experimentally relevant values of $\bar{N} \lesssim 10^4$ [9].

Nevertheless, experiments by Takenaka and coworkers [10–13] and then later by Ahn et al. [14] detected stable $Fddd$ regions in polyisoprene-polystrene (PI-PS) diblock copolymer melts, despite the fact that $\bar{N} \approx 1100$. Figure 1 shows the $Fddd$ (O^{70}) regions in the PI-PS phase diagram [15–17]. This apparent contradiction between experiment and theory was recently resolved [18]. Using field-theoretic simulations (FTSs) , it was shown that, at least for diblock copolymer melts, fluctuations enhance the stability of the $Fddd$ phase with respect to the gyroid and lamellar phases, shifting the $Fddd$ region to a sufficient segregation to maintain its order. It was hypothesized that this stabilization is due to the entropy associated with undulating interfaces, which is omitted by the Landau-Brazovskii calculation due to a truncation of wave vectors.

Since the discovery of $Fddd$ in bulk diblock copolymer melts, it has been observed in thin films [19] and with added minority-type homopolymer [20]. In addition to the PI-PS chemistry, it has also been identified in polystyrene-poly(L-lactide) diblock copolymer melts [21], liquid-crystalline diblock copolymer melts [22], and high-χ miktoarm starblock copolymer melts [23, 24]. As researchers begin to consider $Fddd$ as a candidate morphology, they may very well find that it is relatively common. Indeed, SCFT calculations [25–27] are now routinely predicting the $Fddd$ phase with varying levels of stability. One class of architectures for which it appears particularly stable is the $(AB)_M$ starblock, consisting of

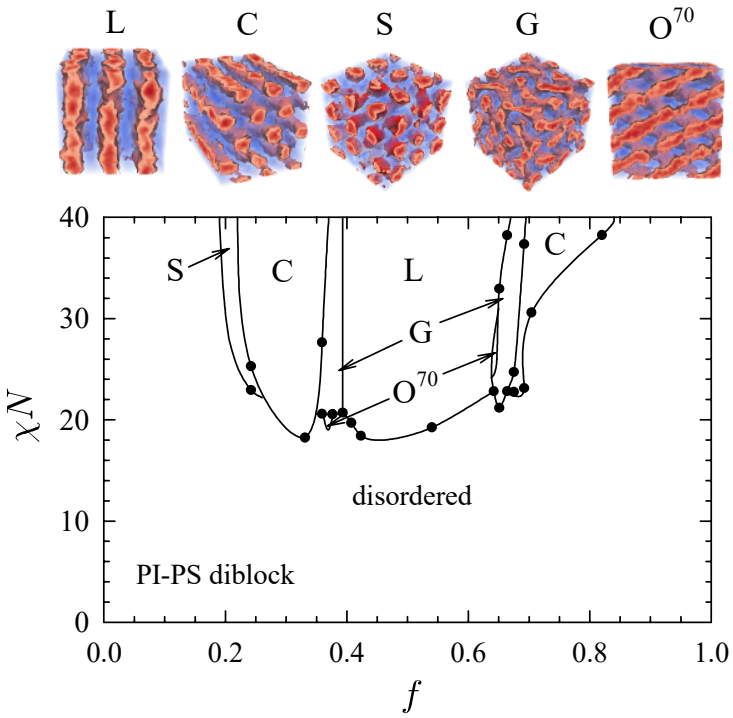


FIG. 1: Phase diagram for PI-PS diblock copolymer melts obtained from a compliment of experiments [15–17]. The images at the top show the domain structure for the ordered lamellar (L), cylindrical (C), spherical (S), gyroid (G), and $Fddd$ (O^{70}) phases obtained from FTSs.

M identical diblock arms joined by their B ends. Even still, it does not extend beyond the weak segregations typically destroyed by fluctuations. Therefore, we apply FTSs to this class of molecules to assess whether $Fddd$ will again survive fluctuation effects as it does for the simple diblock copolymer (i.e., $M = 1$).

FIELD-THEORETIC SIMULATIONS

We model the starblock copolymers using discrete chains with point-like monomers connected by harmonic bonds [28], as illustrated in Fig. 2. The coordinates of the monomers are denoted by $\mathbf{r}_{\alpha,j,i}$, where $\alpha = 1, 2, \ldots, n$ indexes the molecules, $j = 1, 2, \ldots, M$ indexes the arms, and $i = 1, 2, \ldots, N$ indexes the monomers within each arm. The position of the vertex where the M arms are joined is denoted by $\mathbf{r}_{\text{core},\alpha}$. In terms of these coordinates, the

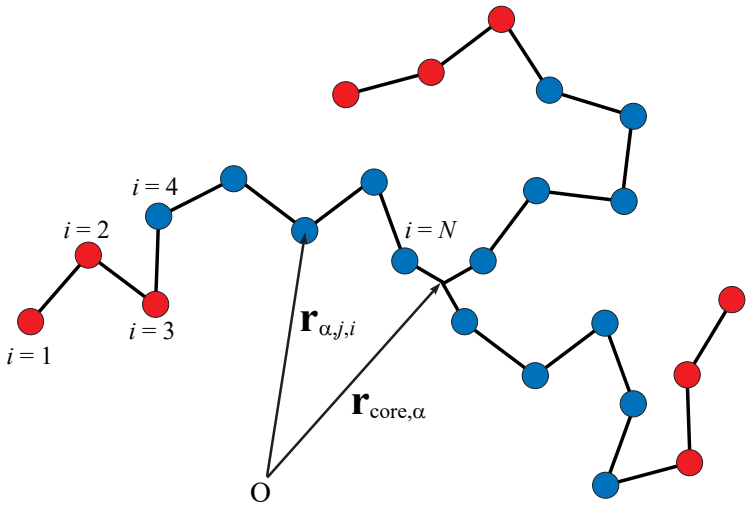


FIG. 2: Schematic diagram of a 3-arm starblock copolymer with $N_A = 3$ and $N_B = 5$. Monomer positions are given by the vectors $\mathbf{r}_{\alpha,j,i}$ and the vertex of the star is denoted by the vector $\mathbf{r}_{\mathrm{core},\alpha}$

.

energy of the bonded interactions is given by the harmonic potentials

$$\begin{aligned}\frac{U_{\mathrm{b}}}{k_B T} &= \frac{3}{2a^2}\sum_{\alpha=1}^{n}\sum_{j=1}^{M}\sum_{i=1}^{N-1}\left|\mathbf{r}_{\alpha,j,i}-\mathbf{r}_{\alpha,j,i+1}\right|^2 \\ &\quad+\frac{3}{a^2}\sum_{\alpha=1}^{n}\sum_{j=1}^{M}\left|\mathbf{r}_{\alpha,j,N}-\mathbf{r}_{\mathrm{core},\alpha}\right|^2 . \end{aligned} \tag{2}$$

The first set of potentials corresponds to *normal* bonds connecting the monomers within each arm, while the second set involves stiffer bonds that connect the M arms together. We regard the latter as *half* bonds since two connected in series are equivalent to a normal bond; this condition is necessary for all the bonds of a triblock copolymer (i.e., $M = 2$) to be identical.

The block copolymer nature of the molecule is invoked by labeling the outer $i = 1, 2, \ldots, N_A$ monomers as type A and the remaining inner monomers as type B. The monomer types are specified by the array γ_i, which takes on values of $+1$ and -1 for A and B monomers, respectively. Given this definition, the standard Flory-Huggins interaction energy can be written as

$$\frac{U_{\mathrm{int}}}{k_B T} = \frac{\rho_0 \chi_b}{4}\int\left(1-\hat{\phi}_-^2\right)d\mathbf{r}, \tag{3}$$

where χ_b is a *bare* interaction parameter and

$$\hat{\phi}_-(\mathbf{r}) = \frac{1}{\rho_0} \sum_{\alpha=1}^{n} \sum_{j=1}^{M} \sum_{i=1}^{N} \gamma_i \delta(\mathbf{r}_{\alpha,j,i} - \mathbf{r}) \tag{4}$$

is the composition of the melt (i.e., A concentration minus B concentration). The model also assumes the melt is incompressible, which is achieved by imposing the constraint

$$\hat{\phi}_+(\mathbf{r}) = 1, \tag{5}$$

where

$$\hat{\phi}_+(\mathbf{r}) = \frac{1}{\rho_0} \sum_{\alpha=1}^{n} \sum_{j=1}^{M} \sum_{i=1}^{N} \delta(\mathbf{r}_{\alpha,j,i} - \mathbf{r}) \tag{6}$$

is the total monomer concentration.

The particle-based partition function for this model is given by

$$Z = \int \exp\left(-\frac{U_\mathrm{b} + U_\mathrm{int}}{k_B T}\right) \delta[\hat{\phi}_+(\mathbf{r}) - 1] d\{\mathbf{r}_{\alpha,j,i}\}, \tag{7}$$

which involves $3nMN$ integrations over the monomer coordinates. In polymer field theory [38–40], the partition function is converted to

$$Z = \int \exp\left(-\frac{H_f}{k_B T}\right) \mathcal{D}W_- \mathcal{D}W_+, \tag{8}$$

where

$$\frac{H_f}{nMk_BT} = -\frac{1}{M} \ln Q + \frac{\chi_b N}{4} + \frac{N}{V} \int \left(\frac{W_-^2}{\chi_b} - W_+\right) d\mathbf{r} \tag{9}$$

is a field-theoretic Hamiltonian that depends on the fields $W_-(\mathbf{r})$ and $W_+(\mathbf{r})$. In addition to the explicit dependence in the integral, it involves the partition function of a single starblock, Q, where the A and B monomers are acted upon by the fields $W_A(\mathbf{r}) = W_+(\mathbf{r}) + W_-(\mathbf{r})$ and $W_B(\mathbf{r}) = W_+(\mathbf{r}) - W_-(\mathbf{r})$, respectively.

To evaluate Q for a single molecule, we fix the i'th monomer of its first arm at position $\mathbf{r}$, which divides the molecule into two independent portions. We then define a partial partition function, $q_i(\mathbf{r})$, for the portion consisting of the outer i monomers of the first arm, which can be solved recursively with

$$q_{i+1}(\mathbf{r}) = h_{i+1}(\mathbf{r}) \int g(R) q_i(\mathbf{r} - \mathbf{R}) d\mathbf{R}, \tag{10}$$

starting from $q_1(\mathbf{r}) = h_1(\mathbf{r})$. Here,

$$g(R) = \left(\frac{3}{2\pi a^2}\right)^{3/2} \exp\left(-\frac{3R^2}{2a^2}\right) \tag{11}$$

is the Boltzmann weight for a normal bond and

$$h_i(\mathbf{r}) = \exp(-W_+(\mathbf{r}) - \gamma_i W_-(\mathbf{r})) \tag{12}$$

is the Boltzmann weight for the field acting on monomer i. Similarly, we define an analogous partial partition function, $q_i^\dagger(\mathbf{r})$, for the remaining portion of the molecule (i.e., the inner $N - i + 1$ monomers of the first arm and the other $M - 1$ arms attached to it). It is again obtained recursively with

$$q_{i-1}^\dagger(\mathbf{r}) = h_{i-1}(\mathbf{r}) \int g(R) q_i^\dagger(\mathbf{r} - \mathbf{R}) d\mathbf{R}, \tag{13}$$

but starting from a more complex initial condition

$$q_N^\dagger(\mathbf{r}) = h_N(\mathbf{r}) \int g_{1/2}(R) q_{\text{arm}}^{M-1}(\mathbf{r} - \mathbf{R}) d\mathbf{R}, \tag{14}$$

where

$$g_{1/2}(R) = \left(\frac{3}{\pi a^2}\right)^{3/2} \exp\left(-\frac{3R^2}{a^2}\right) \tag{15}$$

is the Boltzmann weight for a half bond and

$$q_{\text{arm}}(\mathbf{r}) = \int g_{1/2}(R) q_N(\mathbf{r} - \mathbf{R}) d\mathbf{R} \tag{16}$$

is the partition function for a single arm anchored to position $\mathbf{r}$. Once the partial partition functions are known, the single-molecule partition function is given by

$$Q = \frac{1}{V} \int \frac{q_i(\mathbf{r}) q_i^\dagger(\mathbf{r})}{h_i(\mathbf{r})} d\mathbf{r} = \frac{1}{V} \int q_1^\dagger(\mathbf{r}) d\mathbf{r}. \tag{17}$$

It can be evaluated using any value of i, but it is most convenient to use $i = 1$.

The above equations are solved in $L_x \times L_y \times L_z$ orthorhombic boxes of volume $V = L_x L_y L_z$ with periodic boundary conditions. In order to represent the fields, the boxes are overlaid with $m_x \times m_y \times m_z$ grids of uniform spacing, $\Delta_\nu = L_\nu / m_\nu$, in the $\nu = x$, y, and z directions. Hence, each grid point corresponds to a finite volume of $V_{\text{cell}} = \Delta_x \Delta_y \Delta_z$. The convolution integrals in Eqs. (10), (13), and (16) are solved in Fourier space, where they reduce to simple products [28].

One might expect results to become increasingly accurate as $V_{\text{cell}} \to 0$, but that is not the case. Although the model defines the interactions as contact forces, in practice, the range is dictated by the grid spacings, Δ_ν. Consequently, the number of intermolecular interactions

decreases as V_{cell} is reduced, which lowers the degree of segregation, leading to an ultraviolet divergence [29]. Fortunately, the polymer field theory appears to be renormalizable [30]. As such, the divergence can be removed by expressing results in terms of a renormalized or rather *effective* interaction parameter [18, 31]

$$\chi = z_\infty \chi_b + c_2 (z_\infty \chi_b)^2 + c_3 (z_\infty \chi_b)^3 + \cdots \ , \tag{18}$$

where

$$z_\infty = 1 - \frac{1}{V_{\text{cell}} \rho_0} \sum_{i=-\infty}^{\infty} P_i \tag{19}$$

is the relative number of intermolecular contacts for discrete chains, in the limit of $\chi_b \to 0$ and $N \to \infty$, expressed in terms of

$$P_i = \prod_\nu \frac{\Delta_\nu}{a} \sqrt{\frac{3}{2\pi |i|}} \, \text{erf} \left(\frac{\pi a}{\Delta_\nu} \sqrt{\frac{|i|}{6}} \right), \tag{20}$$

the probability that two monomers, separated by i monomers along the chain contour, occupy the same cell of the grid [32]. The remaining coefficients, c_p for $p = 2, 3, ...$, are determined by a Morse calibration [33–35], where the structure function, $S(k)$, for disordered melts of symmetric diblock copolymer are fit to renormalized one-loop (ROL) predictions [36]. In addition to removing the divergence, this maps our results onto the standard Gaussian chain model [37].

SCFT approximates the free energy by $F = H_f[w_-, w_+]$, where $w_-(\mathbf{r})$ and $w_+(\mathbf{r})$ denote the saddle-point of the Hamiltonian, whereas FTSs instead simulate $H_f[W_-, W_+]$ [38–40]. However, there is a complication that $W_+(\mathbf{r})$ is imaginary valued, which Fredrickson and co-workers handle by performing complex-Langevin FTSs [41–43]. Given that the $W_-(\mathbf{r})$ fluctuations are dominant, we instead invoke a partial saddle-point approximation for $W_+(\mathbf{r})$ [28, 44, 45]. The partial saddle point, $w_+(\mathbf{r})$, is obtained by enforcing the mean-field version of incompressibility,

$$\phi_+(\mathbf{r}) = 1, \tag{21}$$

where

$$\phi_+(\mathbf{r}) = \frac{1}{NQ} \sum_{i=1}^{N} \frac{q_i(\mathbf{r}) q_i^\dagger(\mathbf{r})}{h_i(\mathbf{r})} \tag{22}$$

is the average monomer concentration in an ensemble of noninteracting polymers subjected to the fields. It turns out that $w_+(\mathbf{r})$ is real, which therefore allows us to simulate $H[W_-, w_+]$ using conventional Langevin dynamics.

In the Langevin dynamics, the composition field evolves according to

$$W_-(\mathbf{r};\tau+\delta\tau) = W_-(\mathbf{r};\tau) - \Lambda(\mathbf{r};\tau)\delta\tau + \mathcal{N}(0,\sigma), \tag{23}$$

where

$$\Lambda = \phi_- + \frac{2W_-}{\chi_b} \tag{24}$$

is a forcing term and $\mathcal{N}(0,\sigma)$ provides random numbers from a normal distribution of zero mean and $\sigma^2 = 2\delta\tau/V_{\text{cell}}\rho_0$ variance. The forcing term depends on the average composition in the ensemble of noninteracting polymers, which is given by

$$\phi_-(\mathbf{r}) = \frac{1}{NQ}\sum_{i=1}^{N}\gamma_i\frac{q_i(\mathbf{r})q_i^\dagger(\mathbf{r})}{h_i(\mathbf{r})}. \tag{25}$$

Here, we increment Eq. (23) using the Leimkuhler-Matthews algorithm described in Ref. 46. The partial saddle-point approximation for the pressure field, $w_+(\mathbf{r};\tau)$, is satisfied by solving Eq. (21) at each time step using the Anderson-mixing algorithm detailed in Ref. 28. Computer source code for our FTSs is provided in the SM [47].

RESULTS

Here we examine the homologous $(AB)_M$ block copolymer series for $M = 1$, 2, and 9, the three cases for which complete SCFT phase diagrams (i.e., including $Fddd$ as a candidate phase) have been previously evaluated [25]. To take advantage of previous FTSs for diblock copolymers ($M = 1$) [18], we perform analogous FTSs for the remaining two architectures using the same $N = 90$. Nevertheless, these new simulations are more computational, particularly for $M = 9$, and furthermore the phase diagrams are no longer symmetric about $f = 0.5$. Therefore, we limit our FTSs to the intermediate $\bar{N} = 10^5$ studied in Ref. 18. This choice still provides significant fluctuation corrections but without imposing excessive computational demands.

To locate order-disorder transitions (ODTs), we examine the structure (or scattering) function [48, 49]

$$\frac{S(k)}{\rho_0 N} = \frac{nM}{(\chi_b V)^2}\langle|W_-(\mathbf{k})|^2\rangle - \frac{1}{2\chi_b N}, \tag{26}$$

where $W_-(\mathbf{k}) \equiv \int W_-(\mathbf{r})\exp(-i\mathbf{k}\cdot\mathbf{r})d\mathbf{r}$ and the angle brackets denote an ensemble average. Figure 3 shows results for the $Fddd$ (O^{70}) phase of a 9-arm starblock copolymer at a composition of $f = 0.633$. As the segregation of the ordered phase is gradually reduced, the Bragg

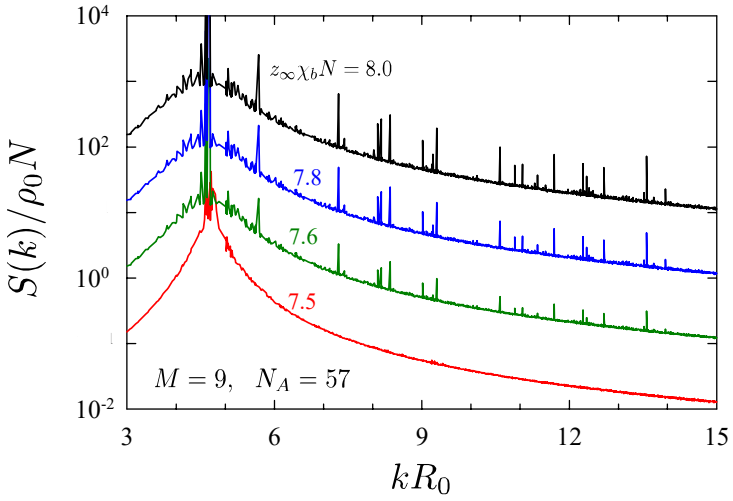


FIG. 3: Structure function, $S(k)$, at a sequence of $z_\infty \chi_b N$ values, calculated for 9-arm starblocks with $N_A = 57$. The upper curves, which are shifted up by integer numbers of decades for clarity, exhibit Bragg peaks signifying the ordered $Fddd$ phase, while the featureless lower curve indicates a disordered morphology.

peaks corresponding to its symmetry decrease and then disappear. This locates the ODT at $z_\infty \chi_b N = 7.55 \pm 0.05$. Although metastablity could, in principle, cause the ordered phase to persist somewhat below the true ODT, previous studies [50, 51] have illustrated that this is not an issue, particularly at the large $\bar{N}$ of our current study. To avoid finite-size effects, the simulations for the L, C, S, G, and O^{70} phases are performed in relatively large boxes containing 3, 6, 27, 8, and 8 unit cells, respectively, as depicted in Fig. 1. The periodicities of the ordered phases are provided by SCFT as previously justified [31, 50, 51], especially for the large $\bar{N}$ of this study.

Order-order transitions (OOTs) are challenging to locate because the simulation box cannot be simultaneously commensurate with the periodicities of both ordered phases. Given the need for separate boxes, free energies are required in order to compare their relative stability. Fortunately, the free energy can be accurately calculated in FTSs by performing thermodynamic integration (TI) [31, 42]. This is done using the composite Hamiltonian,

$$H = \lambda H_f + (1 - \lambda) H_{\text{ec}}, \tag{27}$$

which combines the polymer Hamiltonian in Eq. (9) with the Hamiltonian for an Einstein

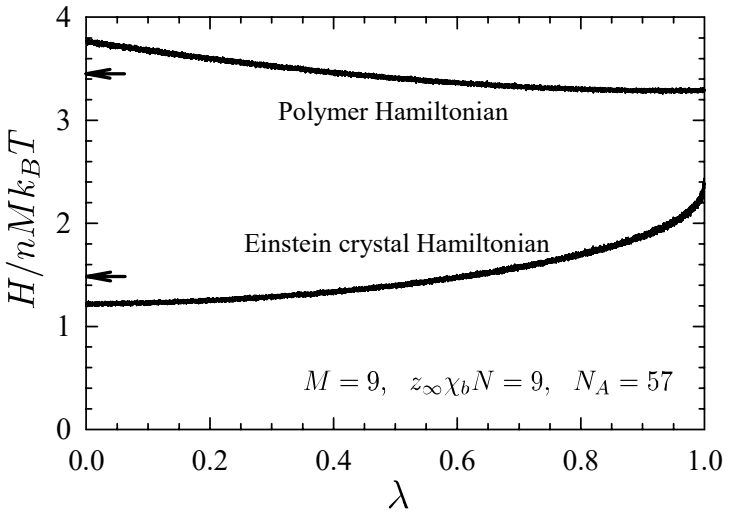


FIG. 4: Samples of the polymer Hamiltonian, H_f, and the Einstein crystal Hamiltonian, $H_{\rm ec}$, during a FTS for the thermodynamic integration of a 9-arm starblock copolymer melt in the $Fddd$ phase at $N_A = 57$ and $z_\infty \chi_b N = 9$. The arrows mark the averages, $\langle H_f \rangle$ and $\langle H_{\rm ec} \rangle$, used in Eq. (30) to evaluate the free energy, F.

crystal of harmonic oscillators,

$$\frac{H_{ec}}{nMk_BT} = \frac{N}{V\chi_b} \int (W_- - W_{\rm ec})^2 d\mathbf{r}. \tag{28}$$

The reference field, $W_{\rm ec}(\mathbf{r})$, is generally set to a previously equilibrated configuration of the ordered phase at similar system parameters. To simulate the composite Hamiltonian, the forcing term in Eq. (23) is set to

$$\Lambda = \lambda \left[\phi_- + \frac{2W_-}{\chi_b} \right] + (1-\lambda) \frac{2[W_- - W_{\rm ec}]}{\chi_b}. \tag{29}$$

During the simulation, H_f and $H_{\rm ec}$ are sampled as λ is gradually incremented from 0 to 1 in steps of $d\lambda$. Once the simulation is complete, the free energy of the block copolymer melt is given by [31]

$$F = \langle H_f \rangle - \langle H_{\rm ec} \rangle \,, \tag{30}$$

where the angle brackets denote averages over the duration of the simulation. Figure 4 shows results for the $Fddd$ phase of a 9-arm starblock melt at $N_A = 57$ and $z_\infty \chi_b N = 9$ using $d\lambda = 5 \times 10^{-6}$. From Eq. (30), we obtain $F/nMk_BT = 3.4477 - 1.4810 = 1.9667$. This free energy is accurate to better than 1 part in 10^4, which is, in fact, necessary for calculating OOTs.

Our OOTs are located by linearly interpolating between free energies evaluated at equal values of $z_\infty \chi_b N$ on opposing sides of the transition; recall that $f = N_A/N$ is restricted to discrete values. Because of the computational cost of the TIs, we reduce the boxes of the L, C, S, G, and O^{70} phases to 3, 4, 8, 1, and 2 unit cells, respectively. Even still, we expect minimal finite-size effects (see Refs. 31 and 51). Because the phases of an OOT need to be simulated in different boxes, they will inevitably require different grid resolutions. Slight imperfections in the renormalization of χ_b can significantly affect free energy comparisons when the cell volumes of the two grids differ by too much [31]. Although this is a relatively minor issue at $\bar{N} = 10^5$, we nevertheless match the V_{cell} values, which is always possible when one of the phases possesses translational symmetry (e.g., the disordered, L, and C phases). Even for the G-O^{70} boundary, where both phases are triply periodic, we still manage to find boxes with V_{cell} values matching to $\lesssim 2\%$.

Figure 5 displays the previous fluctuation-corrected phase diagram for diblocks [18] along with our new diagrams for symmetric triblocks and 9-arm starblocks. In order to compare with the SCFT predictions of Ref. 25, we plot the FTS results in terms of the effective $\chi \approx z_\infty \chi_b + 0.041(z_\infty \chi_b)^2$, as previously calibrated in Ref. 18. The main effect of the fluctuations is to stabilize the disordered phase, which pushes the ODTs to higher segregations, particularly near the mean-field critical points denoted by crosses. $(\chi N)_{\text{ODT}}$ shifts upward by 10% for the diblock and triblock melts, and by 18% for the 9-arm starblock melt. We note that experiments [52] are consistent with our finding of similar-sized shifts for the diblock and triblock ODTs. While these shifts tend to be localized near the critical points, the shift for the starblock melt remains substantial all the way along the large-f side of the ODT. Furthermore, the effect is enhanced near the $Fddd$ region (i.e., $f \approx 0.63$), perhaps because it coincides closely with the mean-field critical point.

The effect of fluctuations on the OOTs is far milder than for the ODTs. Nevertheless, there are some clear trends, particularly at the weaker segregations. The G and O^{70} phases shift toward the L phase, the C phase tends to shift toward the G phase, and the S phase toward the C phase. In all these cases, the shift is toward the phase with the lower average interfacial curvature. It has been suggested that the entropy associated with fluctuations of the internal interfaces favors interfacial curvature [18, 53], as is the case in lyotropic liquid crystals [54]. However, there is one exception; the O^{70} boundaries not only shift toward the L phase but also toward the G phase, despite that the interfaces of G have a higher average

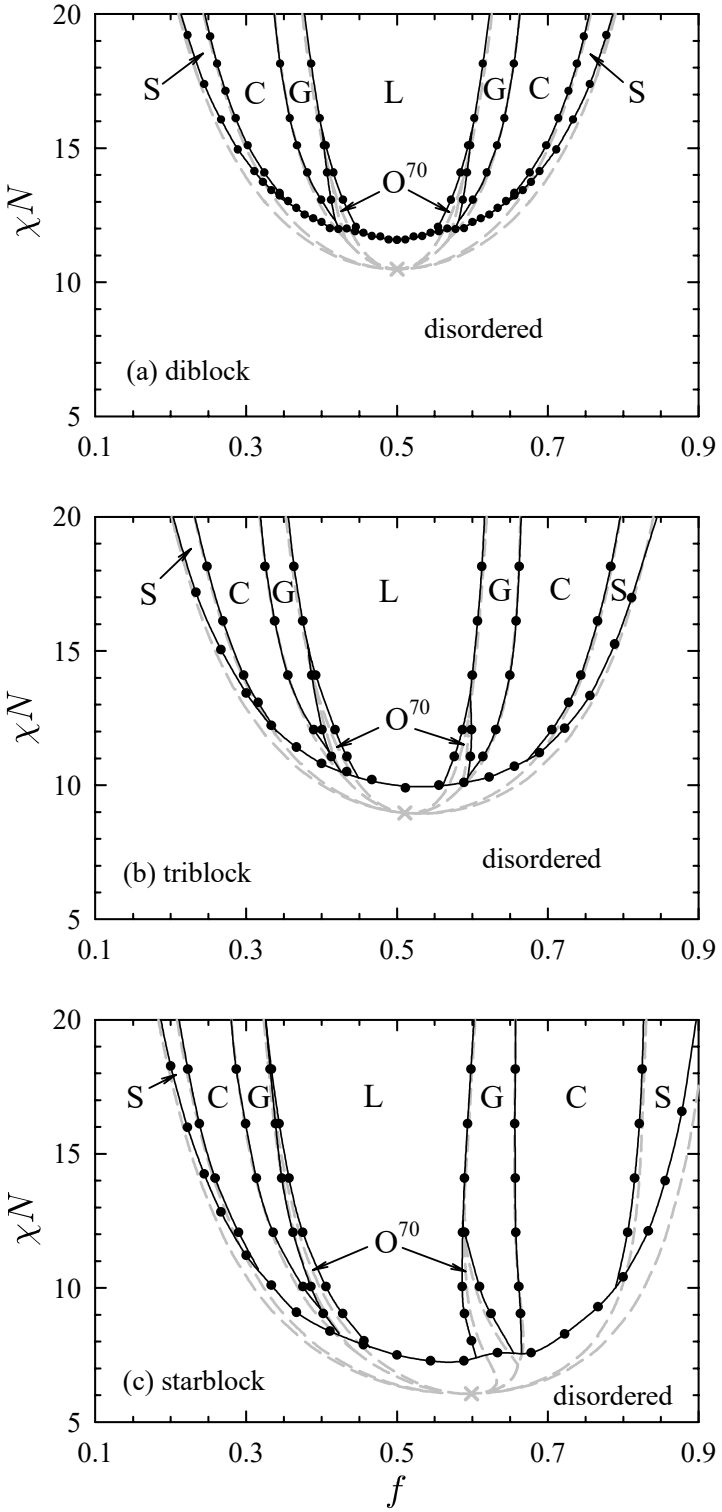


FIG. 5: Phase diagrams for (a) AB diblocks, (b) $(AB)_2$ triblocks, and (c) $(AB)_9$ starblocks, calculated for $\bar{N} = 10^5$ using FTSs. Circles denote the FTS data points and solid curves provide a guide to the eye. For comparison, SCFT predictions for $\bar{N} \to \infty$ are shown with dashed curves, and mean-field critical points are denoted by crosses.

curvature. This implies, not surprisingly, that fluctuation effects on the ordered phases are not solely governed by the average of the interfacial curvature.

The increased stability of the $Fddd$ phase with respect to its ordered neighbors causes the $Fddd$ region to shift toward higher χN relative to the SCFT prediction corresponding to $\bar{N} \to \infty$. Evidently, this shift is sufficient in the case of PS-PI diblock copolymer melts ($\bar{N} \approx 1100$) to prevent the $Fddd$ region from being wiped out by the disordered phase. The question is whether the same will be true for starblock copolymers. On the small-f side of the starblock diagram, SCFT predicts a long and narrow $Fddd$ region that extends toward intermediate segregation. Fluctuations not only increase its width but also extend it to higher segregation. Given that $Fddd$ survives fluctuations in diblock melts, it is a virtual certainty that it will continue to do so for starblock melts. Although SCFT predicts an unusually wide $Fddd$ region on the large-f side of the starblock diagram, it is nevertheless limited to relatively weak segregations. Fluctuations do push the $Fddd$ region toward higher segregation, but only slightly. Considering the enhanced upward shift of the ODT in starblock melts, it seems doubtful that $Fddd$ would survive the level of fluctuations typical of experiments.

DISCUSSION

Until now, the study of fluctuation effects has been almost exclusively limited to diblock copolymer melts. The only fluctuation-corrected phase diagrams for complicated architectures have been based on the Landau-Brazovskii theory, which involves a considerable number of approximations including the cutoff of large wave vectors that prevents small-scale undulations of the internal A/B interfaces. Mayes and Olvera de la Cruz [55] applied the theory to ABA triblock copolymer melts, but they only considered the classical L, C, and S phases. Floudas et al. [56] later applied it to $(AB)_4$ starblock copolymer melts. They considered the gyroid phase but not the $Fddd$ phase. Strangely, though, the G phase in their mean-field and fluctuation-corrected phase diagrams is extraordinarily stable at asymmetric compositions, which contradicts SCFT predictions [25, 57] as well as our current FTSs. It is hard to understand how Landau-Brazovskii predictions for 4-arm starblock melts could differ so much from those of diblock melts [8, 58, 59]. We suspect that there is an issue with the way they handled the higher-order wave vectors required to treat the G phase.

Apart from Landau-Brazovskii calculations, most previous studies of fluctuations are based on conventional particle-based simulations. These are reasonably effective for linear polymers such as diblocks and triblocks, but they become challenging for larger multiblock copolymers. In addition to the increased size, the dynamics of nonlinear polymers is notoriously slow. Particle-based simulations of our 9-arm starblock copolymers, each containing 810 monomers, still remain unfeasible at melt densities. There is also the problem of locating OOTs. Although thermodynamic integration can be applied to particle-based simulations, obtaining the necessary four digits of accuracy is impractical. Indeed, particle-based simulations have yet to produce a complete phase diagram for even the simple diblock architecture.

The FTSs not only remove most of the approximations implemented in Landau-Brazovskii theory [7], they also provide sufficiently accurate free energies to evaluate OOTs, and they can readily handle complicated architectures. On the surface, the computational demands of the $(AB)_M$ starblock appear independent of the number of arms, M. However, our FTSs for the 9-arm starblock are $3\times$ as costly as those for the diblock and triblock, because of an increase in the number of Anderson-mixing iterations required to solve the partial saddle-point approximation. Nevertheless, the relative slow down is far less than it would be for a particle-based simulation.

Our FTSs were able to handle a large number ($N = 90$) of monomers per starblock arm, which has a couple of important advantages. For one, it provides a relatively fine resolution in composition, $f = N_A/N$. More importantly, however, the high degree of polymerization ensures that our phase diagrams are in the universal regime [35, 60]. This happens once N is large enough to produce a sufficient separation between the microscopic length scale (i.e., a) and the polymeric length scale (i.e., $R_0 = aN^{1/2}$). In this regime, the dependence on microscopic details, no matter how many extra parameters that might entail, can be completely absorbed into the effective χ. Indeed, the fact that we use discrete as opposed to continuous Gaussian chains is accounted for by the fact that z_∞ in Eq. (19) is defined with a sum [28] as opposed to an integral [32].

Contrary to particle-based simulations, FTSs are most efficient at large $\bar{N}$ and become increasingly computational as $\bar{N}$ is reduced. Fortunately, there have been major algorithmic advances in recent years [46, 61–63], in addition to the usual hardware improvements, that have sped up FTSs by orders of magnitude. Undoubtedly, there will be more to come. Large-scale FTSs on complicated block copolymer systems are certain to become routine for

$\bar{N} \gtrsim 10^4$. However, some technical issues will need to be resolved in order to go much lower in $\bar{N}$. Fortunately, there is good evidence [31, 64–66] that the SCFT predictions for the equilibrium periodicities of the ordered phases remain accurate to relatively low $\bar{N}$. Otherwise, we would have to develop FTS methods for determining the preferred periodicity of triply-periodic phases (e.g., S, G, and O^{70}), since the current methods can only be applied to phases with translational symmetry (e.g., L and C) [31]. A more serious concern [64] is the renormalization of χ_b in Eq. (18), and so that may need to be improved. Furthermore, the partial saddle-point approximation is bound to become inaccurate. Although the approximation can, in principle, be lifted by applying complex-Langevin FTSs, they suffer from an instability which becomes problematic at low $\bar{N}$ (see the SI of Ref. 67). Nevertheless, FTSs are already immensely successful, and the attention that brings will undoubtedly lead to further advances in expanding their applicability.

SUMMARY

We have calculated fluctuation-corrected phase diagrams for $(AB)_M$ block copolymer melts, calibrated with respect to the standard Gaussian-chain model [37]. Along with previous Landau-Brazovskii calculations for ABA triblocks [55] and $(AB)_4$ starblocks [56], these are the first to explore fluctuation effects beyond those of the simple diblock. Notably, our calculations include both complex network phases, gyroid and $Fddd$. They also avoid the truncation of wave vectors imposed in the Landau-Brazovskii theory, thereby allowing the A/B interfaces to fluctuate. Our calculations do, however, retain the partial saddle-point approximation for the incompressibility constraint, but this is expected to have a negligible effect at the large $\bar{N} = 10^5$ of our current study.

As expected, the most significant effect of fluctuations is to shift the ODT to higher χN. We find that the shift for starblocks ($M = 9$) is more pronounced compared to simple diblocks ($M = 1$) and symmetric triblocks ($M = 2$), not only in the vicinity of the mean-field critical point but also at asymmetric compositions corresponding to stars with long end blocks ($f > 0.5$). The effect of fluctuations on the OOTs is relatively mild, but it is generally consistent with the previous observation [18] that the OOTs shift toward the morphology with less interfacial curvature. This supports the hypothesis that fluctuations favor curved interfaces [18, 53], as is the case for lyotropic liquid crystals [54]. However, we do find one

exception; fluctuations stabilize the $Fddd$ phase with respect to both the lamellar and gyroid phases.

The fact that fluctuations have such a stabilizing effect on the $Fddd$ phase explains how it manages to survive in diblock copolymer melts [10–14, 21], despite the fact that the weak degree of order predicted by SCFT is typically destroyed by fluctuations [5, 6]. Likewise, we expect the $Fddd$ phase to be stable in $(AB)_M$ starblock copolymer melts on the side of the phase diagram where the end blocks form the network domain ($f < 0.5$). However, our calculations suggest that it is unlikely to be stable on the other side where the cores of the starblocks reside in the network domain ($f > 0.5$).

ACKNOWLEDGMENTS

This work was supported by the Natural Sciences and Engineering Research Council (NSERC) of Canada, and computer resources were provided by the Digital Research Alliance of Canada.

---

* Electronic address: mwmatsen@uwaterloo.ca

[1] T. S. Bailey, C. M. Hardy, T. H Epps, III, and F S. Bates, A noncubic triply periodic network morphology in poly(isoprene-b-styrene-b-ethylene oxide) triblock copolymers, Macromolecules **35**, 7007 (2002).

[2] E. W. Cochran and F. S. Bates, Shear-Induced network-to-network transition in a block copolymer melt, Phys. Rev. Lett. **93**, 087802 (2004).

[3] T. H Epps, III, E. W. Cochran, C. M. Hardy, T. S. Bailey, R. S. Waletzko, and F S. Bates, Network phases in ABC triblock copolymers, Macromolecules **75**, 7085 (2004).

[4] T. H Epps, III, E. W. Cochran, T. S. Bailey, R. S. Waletzko, C. M. Hardy, and F S. Bates, Ordered network phases in linear poly(isoprene-b-styrene-b-ethylene oxide) triblock copolymers, Macromolecules **75**, 7085 (2004).

[5] C. T. Tyler and D. C. Morse, Orthorhombic Fddd network in triblock and diblock copolymer melts, Phys. Rev. Lett. **94**, 208302 (2005).

[6] M. W. Matsen, Fast and accurate SCFT calculations for periodic block-copolymer morpholo-

gies using the spectral method with Anderson mixing, Eur. Phys. J. E **30**, 361 (2009).

[7] G. H. Fredrickson and E. Helfand, Fluctuation effects in the theory of microphase separation in block copolymers, J. Chem. Phys. **87**, 697 (1987).

[8] B. Miao and R. A. Wickham, Fluctuation effects and the stability of the Fddd network phase in diblock copolymer melts, J. Chem. Phys. **128**, 054902 (2008).

[9] F. S. Bates, M. F. Schulz, A. K. Khandpur, S. Förster, J. H. Rosedale, K. Almdal, and K. Mortensen, Fluctuations, conformational asymmetry and block copolymer phase behaviour, Faraday Discuss. **98**, 7 (1994).

[10] M. Takenaka, T. Wakada, S. Akasaka, S. Nishitsuji, K. Saijo, H. Shimizu, M. I. Kim, and H. Hasegawa, Orthorhombic Fddd network in diblock copolymer melts, Macromolecules **40**, 4399 (2007).

[11] M. I. Kim, T. Wakada, S. Akasaka, S. Nishitsuji, K. Saijo, H. Hasegawa, K. Ito, and M. Takenaka, Stability of the Fddd phase in diblock copolymer melts, Macromolecules **41**, 7667 (2008).

[12] M. I. Kim, T. Wakada, S. Akasaka, S. Nishitsuji, K. Saijo, H. Hasegawa, K. Ito, and M. Takenaka, Determination of the Fddd phase boundary in polystyrene-block-polyisoprene diblock copolymer melts **42**, 5266 (2009).

[13] Y.-C. Wang, K. Matsuda, M. I. Kim, A. Miyoshi, S. Akasaka, S. Nishitsuji, K. Saijo, H. Hasegawa, K. Ito, T. Hikima, and M. Takenaka, Fddd phase boundary of polystyrene-block-polyisoprene diblock copolymer melts in the polystyrene-rich region, Macromolecules **48**, 2211 (2015).

[14] H. Ahn, C. Shin, B. Lee, and D. Y. Ryu, Phase transitions of block copolymer film on homopolymer-grafted substrate, Macromolecules **43**, 1958 (2010).

[15] S. Förster, A. K. Khandpur, J. Zhao, F. S. Bates, I. W. Hamley, A. R. Ryan, and W. Bras, Complex phase behavior of polyisoprene-polystyrene diblock copolymers near the order-disorder transition, Macromolecules **27**, 6922 (1994).

[16] S. Förster, A. K. Khandpur, J. Zhao, F. S. Bates, I. W. Hamley, A. R. Ryan, and W. Bras, Polyisoprene-polystyrene diblock copolymer phase diagram near the order-disorder transition, Macromolecules **28**, 8796 (1995).

[17] D. A. Hajduk, H. Takenouchi, M. A. Hillmyer, F. S. Bates, M. E. Vigild, and K. Almdal, Stability of the perforated layer (PL) phase in diblock copolymer melts, Macromolecules **30**,

3788 (1997).

[18] M. W. Matsen, T. B. Beardsley, and J. D. Willis, Fluctuation-corrected phase diagrams for diblock copolymer melts, Phys. Rev. Lett. **130**, 248101 (2023).

[19] J. Jung, H.-W. Park, J. Lee, H. Huang, T. Chang, Y. Rho, M. Ree, H. Sugimori, and H. Jinnai, Soft Matter, **7**, 10424 (2011).

[20] Y.-C. Wang, M.-I. Kim, S. Akasaka, K. Saijo, H. Hasegawa, T. Hikima, and M. Takenaka, Fddd structure in polystyrene-block-polyisoprene diblock copolymer/polystyrene homopolymer blends, Macromolecules **49**, 2257 (2016).

[21] X.-B. Wang, T.-Y. Lo, H.-Y. Hsueh, and R.-M. Ho, Double and single network phases in polystyrene-blockpoly(L-lactide) diblock copolymers, Macromolecules **46**, 2997 (2013).

[22] L. Weng, M. Ma, C. Yin, Z.-X. Fei, K.-K. Yang, C. A. Ross, and L.-Y. Shi, Synthesis and self-assembly of silicon-containing azobenzene liquid crystalline block copolymers, Macromolecules **56**, 470 (2023).

[23] T. Isono, R. Komaki, N. Kawakami, K. Chen, H.-L. Chen, C. Lee, K. Suzuki, B. J. Ree, H. Mamiya, T. Yamamoto, R. Borsali, K. Tajima, and T. Satoh, Tailored solid-state carohydrate nanostructures based on star-shaped discrete block co-oligomers, Biomacromolecules **23**, 3978 (2022).

[24] K. Chen, C.-Y. Chen, H.-L. Chen, R. Komaki, N. Kawakami, T. Isono, T. Satoh, D.-Y. Hung, and Y.-L. Liu, Self-assembly behavior of sugar-based block copolymers in the complex phase window modulated by molecular architecture and configuration, Macromolecules **56**, 28 (2023).

[25] M. W. Matsen, Effect of architecture on the phase behavior of AB-type block copolymer melts, Macromolecules **45**, 2161 (2012).

[26] W. Li, K. T. Delaney, and G. H. Fredrickson, Fddd network phase in ABA triblock copolymer melts, J. Polym. Sci., Part B **54**, 1112 (2016).

[27] Y. Qiang and W. Li, Accelerated method of self-consistent field theory for the study of Gaussian ring-type block copolymers, Macromolecules **54**, 9071 (2021).

[28] M. W. Matsen and T. M. Beardsley, Field-theoretic simulations for block copolymer melts using the partial saddle-point approximation, Polymers **13**, 2437 (2021).

[29] M. Olvera de la Cruz, S. F. Edwards, and I. C. Sanchez, Concentration fluctuations in polymer blend thermodynamics, J. Chem. Phys. **89**, 1704 (1988).

[30] P. Grzywacz, J. Qin, and D. C. Morse, Renormalization of the one-loop theory of fluctuations in polymer blends and diblock copolymer melts, Phys. Rev. E **76**, 061802 (2007).

[31] M. W. Matsen, T. M. Beardsley, and J. D. Willis, Accounting for the ultra-violet divergence in field-theoretic simulations of block copolymer melts, J. Chem. Phys. **158**, 044904 (2023).

[32] T. M. Beardsley and M. W. Matsen, Calibration of the Flory-Huggins interaction parameter in field-theoretic simulations. J. Chem. Phys. **150**, 174902 (2019).

[33] J. Glaser, P. Medapuram, and D. C. Morse, Collective and single-chain correlations in disordered melts of symmetric diblock copolymers: Quantitative comparison of simulations and theory, Macromolecules **47**, 851 (2014).

[34] J. Qin and D. C. Morse, Renormalized one-loop theory of correlations in polymer blends, J. Chem. Phys. **130**, 224902 (2009).

[35] J. Glaser, P. Medapuram, T. M. Beardsley, M. W. Matsen, and D. C. Morse, Universality of block copolymer melts, Phys. Rev. Lett. **113**, 068302 (2014).

[36] J. Qin, P. Grzywacz, and D. C. Morse, Renormalized one-loop theory of correlations in disordered diblock copolymers, J. Chem. Phys. **135**, 084902 (2011).

[37] M. W. Matsen, The standard Gaussian model for block copolymer melts. J. Phys.: Condens. Matter **14**, R21 (2002).

[38] G. H. Fredrickson, V. Ganesan, and F. Drolet, Field-theoretic computer simulation methods for polymers and complex fluids, Macromolecules **35**, 16 (2002).

[39] M. W. Matsen, Field theoretic approach for block polymer melts: SCFT and FTS, J. Chem. Phys. **152**, 110901 (2020).

[40] G. H. Fredrickson and K. T. Delaney, Field-theoretic simulations in soft matter and quantum fluids (Oxford University Press, New York, 2023).

[41] V. Ganesan and G. H. Fredrickson, Field-theoretic polymer simulations, Eurphys. Lett. **55**, 814 (2001).

[42] E. M. Lennon, K. Katsov, and G. H. Fredrickson, Free energy evaluation in field-theoretic polymer simulations, Phys. Rev. Lett. **101**, 138302 (2008).

[43] K. T. Delaney and G. H. Fredrickson, Recent developments in fully fluctuating field-theoretic simulations of polymer melts and solutions, Macromolecules **120**, 7615 (2016).

[44] E. Reister, M. Müller, and K. Binder, Spinodal decomposition in a binary polymer mixture: Dynamic self-consistent-field theory and Monte Carlo simulations, Phys. Rev. E **64**, 041804

(2001).

[45] D. Düchs, V. Ganesan, G. H. Fredrickson, and F. Schmid, Fluctuation effects in ternary AB+A+B polymeric emulsions, Macromolecules **36**, 9237 (2003).

[46] B. Vorselaars, Efficient Langevin and Monte Carlo sampling algorithms: The case of field-theoretic simulations, J. Chem. Phys. **158**, 114117 (2023).

[47] See Supplemental Material at [insert URL] for computer source code to evaluate the structure function and to perform thermodynamic integration of the free energy.

[48] M. Müller and F. Schmid, Incorporating fluctuations and dynamics in self-consistent field theories for polymer blends, in *Advanced Computer Simulation Approaches for Soft Matter Sciences II*, edited by C. Holm and K. Binder (Springer-Verlag, Berlin, 2005).

[49] R. K. W. Spencer and M. W. Matsen, Critical point of symmetric binary homopolymer blends, Macromolecules **49**, 6116 (2016).

[50] T. M. Beardsley and M. W. Matsen, Fluctuation correction for the order–disorder transition of diblock copolymer melts, J. Chem. Phys. **154**, 124902 (2021).

[51] T. M. Beardsley and M. W. Matsen, Well-tempered metadynamics applied to field-theoretic simulations of diblock copolymer melts, J. Chem. Phys. **157**, 114902 (2022).

[52] S.-M. Mai, W. Mingvanish, S. C. Turner, C. Chaibundit, J. P. A. Fairclough, F. Heatley, M. W. Matsen, A. J. Ryan, and C. Booth, Microphase-separation behavior of triblock copolymer melts. Comparison with diblock copolymer melts, Macromolecules **33**, 5124 (2000).

[53] M. Yadav, F. S. Bates, and D. C. Morse, Network model of the disordered phase in symmetric diblock copolymer melts. Phys. Rev. Lett. **121**, 127802 (2018).

[54] D. C. Morse, Entropy and fluctuations of monolayers, membranes, and microemulsions, Curr. Opin. Colloid Interface Sci. **2**, 365 (1997).

[55] A. M. Mayes and M. Olvera de la Cruz, Concentration fluctuation effects on disorder-order transitions in block copolymer melts. J. Chem. Phys. **95**, 4670 (1991).

[56] G. Floudas, S. Pispas, N. Hadjichristidis, T. Pakula, and I. Erukhimovich, Microphase Separation in star block copolymers of styrene and isoprene. Theory, experiment, and simulation, Macromolecules **29**, 4142 (1996).

[57] M. W. Matsen and M. Schick, Microphase separation in starblock copolymer melts. Macromolecules **27**, 6761 (1994).

[58] I. W. Hamley and V. E. Podneks, On the Landau-Brazovskii theory for block copolymer melts,

Macromolecules **30**, 3701 (1997).

[59] P. D. Olmsted and S. T. Milner, Analytical weak-segregation theory of bicontinuous phases in diblock copolymers, J. Phys. II (France) **7**, 249 (1997).

[60] J. Glaser, J. Qin, P. Medapuram, M. Müller, and D. C. Morse, Test of a scaling hypothesis for the structure factor of disordered diblock copolymer melts, Soft Matter **113**, 11310 (2012).

[61] K. T. Delaney and G. H. Fredrickson, Polymer field–theory simulations on graphics processing units, Comput. Phys. Commun. **184**, 2102 (2013).

[62] T. M. Beardsley, R. K. W. Spencer, and M. W. Matsen, Computationally efficient field-theoretic simulations for block copolymer melts, Macromolecules **52**, 8840 (2019).

[63] D. Yong and J. U. Kim, Accelerating Langevin field-theoretic simulation of polymers with deep learning, Macromolecules **55**, 6505 (2022).

[64] B. Vorselaars, P. Stasiak and M. W. Matsen, Field-theoretic simulation of block copolymers at experimentally relevant molecular weights. Macromolecules **48**, 9071 (2015).

[65] P. Medapuram, J. Glaser, and D. C. Morse, Universal phenomenology of symmetric diblock copolymers near the order-disorder transition, Macromolecules **48**, 819 (2015).

[66] T. Ghasimakbari and D. C. Morse, Order-disorder transitions and free energies in asymmetric diblock copolymers, Macromolecules **53**, 7399 (2020).

[67] D. L. Vigil, K. T. Delaney, and G. H. Fredrickson, Quantitative comparison of field-update algorithms for polymer SCFT and FTS, Macromolecules **54**, 9804 (2021).